

Nonvolatile Static Random Access Memory (NV-SRAM) Using Magnetic Tunnel Junctions with Current-Induced Magnetization Switching Architecture

Shuu'ichirou Yamamoto^{1,4} and Satoshi Sugahara^{2,3,4}

¹Department of Information Processing, Tokyo Institute of Technology, Yokohama 226-8502, Japan

²Imaging Science and Engineering Laboratory, Tokyo Institute of Technology, Yokohama 226-8503, Japan

³Department of Electronics and Applied Physics, Tokyo Institute of Technology, Yokohama 226-8502, Japan

⁴CREST, Japan Science and Technology Agency, Kawaguchi 332-0012, Japan

Abstract:

We propose and computationally analyze a nonvolatile static random access memory (NV-SRAM) cell using magnetic tunnel junctions (MTJs) with magnetic-field-free current-induced magnetization switching (CIMS) architecture. A pair of MTJs connected to the storage nodes of a standard SRAM cell with CIMS architecture enables fully electrical store and restore operations for nonvolatile logic information. The proposed NV-SRAM is expected to be a key component of next-generation power-gating logic systems with extremely low static-power dissipation.

1. Introduction

In recent years, power dissipation has been one of the most important concerns for highly integrated advanced complementary metal-oxide-semiconductor (CMOS) logic circuits, since it constrains their performance and the degree of device integration. In general, power dissipation in CMOS logic circuits can be divided into two components, dynamic and static power. The former is caused by on-current passing through CMOS logic gates due to logic operations, and the latter by leakage current in the CMOS gates during standby mode. The magnitude of the leakage current in CMOS gates is exponentially small in comparison with the on-current. However, static power dissipation gives rise to severe problems for CMOS logic circuits with very large scale integration. Recently proposed power-gating architecture based on multithreshold voltage CMOS (MTCMOS) technology is expected to be very effective at reducing static power dissipation in CMOS logic circuits.¹⁻⁷ In this type of architecture, logic circuits on a chip are partitioned into several circuitry domains, so-called power domains that are electrically separated from power supply lines and/or ground lines by sleep transistors, and these domains can be shut down during standby periods. Static power is thereby drastically reduced. A key technology for realizing power-gating systems is the backup of logic information in power domains. Static random access memory (SRAM) and its

related latch circuits including a flip-flop (FF) play an essential role in data latches for high-speed logic circuits. However, these memory devices cannot be shut down without losing information. In addition, SRAM and FF dissipate static power during data retention owing to the presence of leakage current in their constituent CMOS gates. The recently developed embedded SRAM array in a microprocessor has the capability of entering "sleep" standby mode, thereby reducing the magnitude of supply voltage to the minimum value required for the memory cells to retain data.³⁻⁶ However, this technique cannot reduce the static power to zero. One approach to realizing power-gating architecture for circuitry domains that require no power during standby is to transfer key information from the SRAM/FF in the power domains to a backup SRAM/FF placed in continuously powered circuitry before the power domains are shut down.^{3,4,7} However, this architecture requires an inconvenient and complicated access procedure for data transfer through a signal bus line or a specially added one-to-one data transfer line. The limited data transfer rates of bus lines and the complex interconnected wiring of one-to-one data transfer lines are not suitable for power-gating systems with power domains that are frequently switched on and off. Another approach is to use nonvolatile memory such as ferroelectric random access memory (FeRAM) and magnetoresistive random access memory (MRAM) in power domains instead of SRAM and FF. However, these memory devices cannot easily replace SRAM and FF, since the operation speed of these devices cannot easily satisfy the requirements of SRAM and FF applications. Therefore, nonvolatile SRAM (NV-SRAM) and nonvolatile FF (NV-FF) with high performance comparable to that of standard SRAM and FF are indispensable for power-gating logic systems.

One of the most important applications of NV-SRAM and NV-FF is in nonvolatile power-gating processors as shown in Fig.1, which can be realized by applying NV-FF and NV-SRAM to important memory devices, such as the module configuration register, general purpose register, cache memory, and local storage memory. NV-SRAM and NV-FF can be shut down without losing data, and thus can enable efficient power-gating with domains that require no power during standby, leading to a drastic reduction of static power dissipation. Each power domain of the processor has the ability to execute a fast state transition between normal operation mode and "shutdown" mode, since NV-SRAM and NV-FF require no data transfer to backup memory devices. Using a power management unit to control the sleep transistors of the power domains, NV-SRAM and NV-FF make it possible to establish effective run-time power gating. Combined with a high-density nonvolatile memory (such as MRAM) as the main memory, a dynamic power-gating computing system can be established, as shown in the figure. It should be noted that the nonvolatile feature of the main memory is also beneficial, since it requires no program/data loadings from external memory (such as a hard disk drive), when the computing system restarts to execute the suspended operation of a previous powered-on period.

NV-SRAM utilizing a standard SRAM cell with ferroelectric capacitors or resistive switching devices has already been demonstrated.⁸⁻¹¹ Magnetic tunnel junctions (MTJs) are an alternative promising candidate as a nonvolatile storage element for NV-SRAM. The Recent development of very high tunneling magnetoresistance (TMR) ratios at room temperature¹²⁻¹⁴ is useful feature for MRAM¹⁵⁻¹⁷ and would also be applicable to NV-SRAM. Although NV-SRAM cells using MTJs have already been reported,¹⁸⁻²⁰ they employ a magnetic field for magnetization switching of the MTJs, induced by current through the interconnections of the circuit. Thus, they potentially have serious problems for programming power, and programming disturbs (that is a technical term of failure mechanism for programming error). On the other hand, magnetic-field-free current-induced magnetization switching (CIMS) technology²¹⁻²⁶ allows fully electrical programming for MTJs, and it is expected that the problems of programming power and disturbs can be solved by CIMS technology. The circuit configuration of the above-described NV-SRAM cells using field-induced magnetization switching (FIMS)¹⁸⁻²⁰ cannot be applied to CIMS architecture, since MTJs in the cells using FIMS are placed in their inverter loop, and thus bidirectional current (which is required for CIMS from parallel to antiparallel magnetization and from antiparallel to parallel magnetization) is hardly generated.

In this paper, we propose and computationally analyze a new NV-SRAM cell using a pair of MTJs with CIMS architecture for fully electrical nonvolatile information storage.

2. Proposed NV-SRAM cell

Figure 2(a) shows the proposed NV-SRAM cell. The cell consists of two cross-coupled CMOS inverters with two pass transistors and a pair of MTJs. The cross-coupled inverters act as a bistable circuit; that is, a circuit that has two stable operating states that correspond to the logic information of 0 (a low voltage level, hereafter denoted by L) and 1 (a high voltage level, hereafter denoted by H). The pass transistors connected to the two storage nodes Q and /Q act as data-access transistors. The two MTJs are also connected to the two storage nodes. Logic information in the bistable circuit can be electrically stored as a magnetization configuration of these MTJs by CIMS using a pulse signal applied to the control (CTRL) line shown in Fig. 2(a), and thus the NV-SRAM cell can be powered off during shutdown mode without losing logic information. When the cell returns to the normal SRAM operation mode, the information stored in the MTJs is quickly restored to the corresponding logic state of the bistable circuit. This can be achieved as a result of the difference in the charging speed of the two storage nodes, owing to the asymmetry of resistances of the two MTJs. Note that NV-latch and NV-FF cells can be realized by connecting capacitive or resistive nonvolatile memory elements to the storage nodes of an inverter loop.²⁷⁻²⁹ However, there have also not been yet any reports on NV-latch and NV-FF using MTJs with CIMS architecture.

NV-latch and NV-FF cells can also be easily configured in the same manner as the present NV-SRAM cell using a pair of MTJs. Figure 2(b) shows a positive edge triggered master-slave nonvolatile delay-FF (NV-DFF) that consists of a conventional latch and an NV-latch, as indicated in the figure.

3. Device modeling and simulation procedure

In order to analyze the circuit operation of the proposed NV-SRAM cell, we developed a SPICE (simulation program with integrated circuit emphasis) macromodel of an MTJ device including CIMS.³⁰ The fundamental circuit of our model consists of variable resistors and current-controlled ideal switches. The concept of the circuit model is similar to the model reported by Zhao et al.³¹ However, our MTJ model can closely fit the electrical characteristics of recently developed CoFeB/MgO/CoFeB MTJs,¹⁴ and includes CIMS phenomenon (discussed later). Figures 3(a) and 3(b) show the current-voltage and resistance-voltage characteristics of the developed MTJ model, respectively. The positive-current direction is defined by the direction from the free layer to the pinned layer in the MTJ model (denoted by f and p, respectively, in the inset of Fig. 3(a)). The junction resistances $R_{ap}(0)$ and $R_p(0)$ of the MTJ model in the antiparallel and parallel magnetization configurations at zero bias voltage were set to 16.7 and 8.33k Ω , respectively, resulting in a TMR ratio ($=[R_{ap}(0)-R_p(0)]/R_p(0)$) of 100%. This relatively high TMR ratio is easily achieved by recently developed MgO tunnel barrier technology.¹²⁻¹⁴ MgO-based MTJs with a high TMR ratio showed nonlinear tunneling-type (Simons' formula type) current-voltage characteristics in the antiparallel magnetization configuration, and ohmic-like current-voltage characteristics in the parallel magnetization configuration.^{14,21,22} Therefore, R_{ap} and R_p can be phenomenologically modeled as follows:

$$R_{ap}(V_{MTJ}) = R_p(0) + [R_{ap}(0) - R_p(0)] \cdot \exp\left(-\frac{|V_{MTJ}|}{V_{half}/\ln 2}\right), \quad (1)$$

$$R_p(V_{MTJ}) = R_p(0), \quad (2)$$

where V_{MTJ} and V_{half} are the bias voltage applied to the device and the V_{MTJ} value when the TMR ratio is reduced to half its original value, respectively. This model can reproduce the finding that R_{ap} is asymptotically close to R_p at higher voltages. We compared our model with the experimentally obtained electrical characteristics of a MgO-based MTJ reported in ref. 14. Our model reproduced the experimental results within an absolute error of 1.5% and a standard error of 0.9%.

In the following simulations, a V_{half} value of 0.5V was used¹² unless otherwise stated. The previously noted R_p and R_{ap} values were set so that currents through MTJ₁ and MTJ₂ exceed critical currents I_{CF} and I_{CR} at the desired bias voltage. I_{CF} for CIMS from the antiparallel to parallel magnetization configuration and I_{CR} from the parallel to antiparallel magnetization configuration were set to 30 and -30 μ A, respectively. (Their corresponding current density J_C is 1×10^6 A/cm²,^{14,21}

when the junction area is $0.003\mu\text{m}^2$.) In general, the switching speed of CIMS depends on the current density through the MTJ. A lower current density causes a lower switching speed and requires a wider pulse duration. This phenomenon was included in our SPICE macromodel as a "switching delay". The switching delay is realized by timer circuitry, which consists of a voltage comparator and a delay circuit, and it can be set to the desired value by changing the resistance-capacitance product of the delay circuit. In this paper, the switching delay was set at a constant value of 1ns ,²⁶ that is, shorter than the pulse width of the store signal applied to the MTJs through the CTRL line by a sufficient amount. In actual usages, the pulse width of the store signal may be prolonged to guarantee a successful store operation. In this paper, the sweep rate of the restore signal (V_{SP}) was set to 1V/ns . The rate should be chosen to assure successful restore operation, and a lower rate is preferable for achieving this. Note that a large store-signal pulse width and a low restore-signal sweep rate do not degrade the performance of normal SRAM operation. Figure 3(c) shows the simulated response of the MTJ current when an alternating triangle voltage V_{MTJ} is applied. CIMS hysteresis is clearly reproduced by our model without unwanted switching noise.

Operation of the proposed cell including its transition response was analyzed by HSPICE with a $0.07\mu\text{m}$ gate-length technology model.³² The gate lengths(L)/widths(W) of n-channel and p-channel MOSFETs were set to $0.07/1\mu\text{m}$ and $0.07/1.5\mu\text{m}$, respectively. The wide gates were used in order to readily achieve CIMS. Although the gate width can be reduced by optimizing the circuit design, a drastic reduction of the gate width requires a reduction of J_{C} to achieve CIMS. This is the same situation as the case for MRAM using CIMS (spin RAM or spin transfer torque RAM).^{21,22} When a relatively low J_{C} value (such as $5\times 10^5\text{A/cm}^2$) and a small MTJ (such as $0.001\mu\text{m}^2$) are assumed, a narrow gate width with a W/L ratio of unity is applicable.³³

The threshold voltages V_{thp} and V_{thn} of the p-channel and n-channel MOSFETs are -0.21 and 0.19V , respectively. The supply voltage V_{SP} of the CMOS inverters in the cell during normal SRAM operation was set to 1V . In our simulation, the CTRL line is grounded, floating of the CTRL line or applying a small voltage to the CTRL line can also be appropriate to reduce unwanted leakage current through the MTJs of the NV-SRAM cell during normal SRAM operation. (A related discussion is presented in section 4.3.)

4. Results and discussion

4.1. Store operation of NV-SRAM

Operation of the NV-SRAM cell during normal SRAM operation proceeds in the same manner as an ordinary SRAM. The store operation can be performed only by applying a pulse signal to the CTRL line, when the bistable circuit is in one of the stable logic states. Figures 4(a) and 4(b) show schematic illustrations of the store operation of the proposed NV-SRAM cell, where the CTRL

line is at levels L and H, respectively, and Fig. 4(c) shows that of the restore operation (discussed latter). In Figs. 4(a) and 4(b), the stored information of node Q is at level H and that of node /Q is at level L. The magnetization configuration of both MTJ₁ and MTJ₂ is antiparallel, which is realized by the operation of data reversal of the bistable circuit during normal SRAM operation, as shown in the last part of the time chart of Fig. 5. (Note that R_{J2} (R_{J1}) shown in Fig. 5(a) (Fig. 5(b)) is less than R_{ap}(0).) This is due to the bias dependence of R_{ap} expressed by eq. (1). The store operation is independent of the initial magnetization configurations of MTJ₁ and MTJ₂, as described later. I_{J1} and I_{J2} in Fig. 4 represent currents through MTJ₁ and MTJ₂, respectively. The positive-current direction of I_{J1} and I_{J2} is the direction from the free layer to the pinned layer of MTJ₁ and MTJ₂, respectively, as described previously. It should be noted that in the parallel (antiparallel) magnetization configuration, a negative (positive) current induces CIMS but a positive (negative) current does not, as shown in Figs. 3(a) and 3(b). Figure 5(a) shows simulated waveforms of the NV-SRAM cell, where the time evolution of voltages on the WL, VSP, and CTRL lines, and of voltages V_Q and V_{/Q} at nodes Q and /Q, respectively, are plotted. Changes in the magnetization configurations of MTJ₁ and MTJ₂ are also respectively shown by R_{J1} and R_{J2} in the figure. Before the application of a signal to the CTRL line, negative I_{J1} flows since the CTRL line is grounded and V_Q=H [Fig. 4(a)], and thus R_{J1} remains at R_{ap}. R_{J2} also maintains its initial value, since I_{J2} cannot flow through MTJ₂ because V_{/Q}=L [Fig. 4(a)]. When a store signal on the CTRL line pulls up to level H, positive I_{J2} can flow [see Fig. 4(b)] and R_{J2} simultaneously decreases to R_{ap}(V_{MTJ}=H), as shown in Fig. 5(a). Since I_{J2} is designed to exceed I_{CF} under this bias condition, the magnetization configuration of MTJ₂ switches to parallel after the switching delay, resulting in R_{J2}=R_p. In contrast, the magnetization configuration of MTJ₁ does not vary because V_Q=H, although the resistance R_{J1} increases from R_{ap}(V_{MTJ}=H) to R_{ap}(V_{MTJ}=0) during the application of the CTRL signal, as shown in Fig. 5(a). As a result of the application of the store pulse to the CTRL line, the node information of V_Q=H is transferred into MTJ₁ as the antiparallel magnetization configuration (R_{J1}=R_{ap}), and the node information of V_{/Q}=L is transferred into MTJ₂ as the parallel magnetization configuration (R_{J2}=R_p). It should be noted that if R_{J1}=R_p before the application of a store pulse, negative I_{J1} that exceeds I_{CR} causes CIMS, and thus R_{J1} changes from R_p to R_{ap}. However, if R_{J2}=R_p in the initial state, positive I_{J2} induced by a CTRL pulse does not cause CIMS, and thus R_{J2} does not change. Therefore, the store operation is independent of the initial magnetization configurations of MTJ₁ and MTJ₂. When V_Q=L and V_{/Q}=H, these logic data are also transferred into MTJ₁ and MTJ₂ via the mechanism described above, as shown in Fig. 5(b).

4.2. Restore operation of NV-SRAM

The restore operation to return to a normal SRAM operation mode is also simple. The VSP line connected to INV₁ and INV₂ for power supply is pulled up, while the WL line is maintained at

level L. Figure 4(c) schematically shows the charge and discharge current flows with respect to storage nodes Q and /Q. In this figure, C_{s1} , C_{g1} , C_{s2} , and C_{g2} represent parasitic capacitances at nodes Q and /Q, which consist of wiring, gate-bulk overlap, and gate-source overlap capacitances in the p-channel and n-channel MOSFETs (M_{L1} , M_{L2} , M_{D1} , and M_{D2}) of INV_1 and INV_2 . V_Q and $V_{/Q}$ at storage nodes Q and /Q are given by

$$V_Q = \frac{C_{s1}}{C_{sg1}} V_{SP} + \int \frac{1}{C_{sg1}} (I_{L2} - I_{D2} - I_{J1}) dt, \quad (3)$$

$$V_{/Q} = \frac{C_{s2}}{C_{sg2}} V_{SP} + \int \frac{1}{C_{sg2}} (I_{L1} - I_{D1} - I_{J2}) dt, \quad (4)$$

where $C_{sg1} = C_{s1} + C_{g1}$ and $C_{sg2} = C_{s2} + C_{g2}$. I_{L1} (I_{L2}) and I_{D1} (I_{D2}) represent the charge and discharge currents with respect to node Q (/Q) through the p-channel and n-channel MOSFETs of INV_1 (INV_2), respectively. Simulated waveforms exhibited during the restore operation are also shown in Fig. 5(a), and the details of time evolution of V_Q , $V_{/Q}$, $V_{SP} - V_Q$, and $V_{SP} - V_{/Q}$ are shown in Fig. 6(a), where V_{SP} increases from 0 to level H. Figure 6(b) shows the TMR ratio of MTJ_1 during the restore operation.

In the initial stage of the restore operation (region I denoted in Fig. 6(a)), the charging of nodes Q and /Q is governed by the first terms of eqs. (3) and (4), and nodes Q and /Q are simultaneously discharged by I_{J1} and I_{J2} , respectively. In this region, the charge and discharge currents I_{L1} , I_{L2} , I_{D1} , and I_{D2} are negligible, because all the MOSFETs are in a cut-off condition. Since it can be assumed that $C_{s1} \approx C_{s2}$ and $C_{g1} \approx C_{g2}$ owing to the device and circuit symmetries and to the similar bias conditions of both inverters INV_1 and INV_2 during this stage, both V_Q and $V_{/Q}$ gradually increase. However, V_Q is always higher than $V_{/Q}$. This is due to the difference in the discharge rate between Q and /Q, which is because $R_{J1} (=R_{ap}) > R_{J2} (=R_p)$, and thus $I_{J1} < I_{J2}$. Note that although the TMR ratio of MTJ_1 decreases with increasing V_Q because of its antiparallel magnetization configuration, the TMR ratio is not significantly degraded in region I. (V_Q and the TMR ratio only increases to 0.04V and decreases to 95%, respectively, at the boundary between regions I and II shown in Fig. 6.) After $V_{SP} - V_{/Q}$ and $V_{SP} - V_Q$ exceed the threshold voltages $|V_{thp2}|$ and $|V_{thp1}|$ ($=|V_{thp2}|$) of M_{L2} and M_{L1} , respectively, nodes Q and /Q are also charged by currents I_{L1} and I_{L2} derived from M_{L1} and M_{L2} , respectively [region II in Fig. 6(a)]. During this stage, the operating points of M_{L1} and M_{L2} are in their saturation region, and thus I_{L1} and I_{L2} are governed by gate bias voltages V_Q and $V_{/Q}$, respectively. Owing to the increase in V_Q , the TMR ratio of MTJ_1 is reduced to 77% at the boundary between regions II and III, as shown in Fig. 6(b). However, this TMR value is still sufficient to maintain the relation $I_{J1} < I_{J2}$. Therefore, V_Q is higher than $V_{/Q}$. As a result, the relation $V_{SP} - V_{/Q} > V_{SP} - V_Q$ is maintained, which yields the relation of $I_{L2} > I_{L1}$. This accelerates the charging of node Q, and the voltage difference between V_Q and $V_{/Q}$ is enhanced. Eventually, V_Q becomes higher than the threshold voltage V_{thn1} of M_{D1} . Thus, M_{D1} is turned on, while M_{L1} is turned off [region III in Fig. 6(a)]. Namely, node /Q is discharged by M_{D1} , and $V_{/Q}$ is further reduced. This

leads to a further increase in the charging of V_Q by M_{L2} , and thus M_{D2} cannot be switched on. During this stage, the TMR ratio of MTJ_1 decreases to $\sim 60\%$. However, the reduction of the TMR ratio has no serious impact on the restore operation, since the current drive capabilities of INV_1 and INV_2 become higher than those of MTJ_1 and MTJ_2 in region III, and an initial complementary push-pull operation of INV_1 and INV_2 is established; that is, V_Q and $V_{/Q}$ are in a bistable condition governed by the two inverters, although V_Q does not reach level H. Subsequently, $V_{/Q}$ rapidly approaches level L, and V_Q increases to level H with increasing V_{SP} [region IV in Fig. 6(a)]. The operating points of M_{D1} and M_{L2} enter their linear region. Finally, the feedback loop with the bistable condition of $V_Q \approx H$ (V_Q is lower than level H owing to leakage current through MTJ_1 or MTJ_2 , as discussed later) and $V_{/Q} = L$ is established, which correspond to the information stored in MTJ_1 and MTJ_2 . After the restore operation, the normal mode of SRAM operation is possible.

4.3. Effect of MTJ on normal SRAM operation

A disadvantage of the proposed NV-SRAM cell is the flow of current between the level H storage node and the grounded CTRL line through MTJ_1 or MTJ_2 during normal SRAM mode operation. This leakage current results in excess power dissipation. The circuit current I_{CELL} through the NV-SRAM cell can be defined by $I_{L1} + I_{L2}$ which include the leakage current induced by MTJ_1 or MTJ_2 , is shown in Fig. 5(a). For the retention of data during the normal operation mode, the NV-SRAM cell requires an I_{CELL} value of $87.6\mu A$. Note that it decreases to $0.14\mu A$ when MTJ_1 and MTJ_2 are decoupled from nodes Q and $/Q$, respectively. The maximum value of I_{CELL} is $451\mu A$, which is caused by a normal SRAM operation of data reversal, owing to short circuit currents passing through the inverters. As shown in the last part of the time chart in Fig. 5, the operation of data reversal induces CIMS for one of the MTJs with the parallel magnetization configuration. As a result, both R_{J1} and R_{J2} develop the antiparallel magnetization configuration during normal operation mode (subsequent to the first reversal of data stored in the inverter loop). Obviously, a high R_{ap} value can reduce the unwanted leakage current passing through MTJ_1 or MTJ_2 , and a high V_{half} value is also effective at reducing the leakage current. However, since an increase in R_{ap} with a high V_{half} value requires a high bias for CIMS, the R_p and V_{half} values must be carefully optimized in view of the trade-off between the leakage current in normal operation mode and the bias required for CIMS. Note that although the parallel magnetization configuration in MTJ_1 or MTJ_2 is established only during the period following the restore operation but prior to the first reversal of data, as shown in Fig. 5, this situation has no serious problems. Since the storage node connected to the MTJ with the parallel magnetization configuration is always at level L, no serious leakage current is generated.

The disadvantage of leakage current through MTJ_1 and MTJ_2 can be easily overcome by introducing selector transistors between the storage nodes (or CTRL line) and the MTJs, as shown in Fig. 7(a). The inverter loop of the NV-SRAM cell can be electrically separated from the MTJs by the

selector transistors. Thus, the MTJs have no effect on the operation speed and the power dissipation during normal SRAM operation. Another interesting challenge is to utilize a pair of spin transistors, such as a pair of the spin-MOSFETs,³⁴⁻³⁶ instead of the pair of MTJs, as shown in Fig. 7 (b). Their magnetization-configuration-dependent unique transistor behavior is also suitable for NV-SRAM and NV-FF operations. It is worth noting that the circuit configuration of a selector transistor with the MTJ shown in Fig. 7(a) acts as a spin transistor, referred to as a pseudo-spin-MOSFET,^{37,38} in which its current drive capability can be modified by the magnetization configuration of the MTJ.

5. Conclusions

We propose and computationally analyze an NV-SRAM cell using MTJs with magnetic-field-free CIMS architecture. A pair of MTJs connected to the storage nodes of a standard SRAM cell with CIMS architecture make it possible to execute fully electrical store and restore operations for nonvolatile logic information. The proposed NV-SRAM technology using MTJs with CIMS can be applied to NV-latch and NV-FF, and these nonvolatile devices are expected to be important key components for power-gating logic systems of future high-performance and low-power integrated circuits.

Acknowledgment

The authors would like to thank Professors H. Maejima and H. Munekata of Tokyo Institute of Technology, Professor K. Inomata of National Institute for Materials Science, and Professor M. Tanaka of the University of Tokyo for fruitful discussions and encouragement. This work was partly supported by a Grant-in-Aid for Scientific Research from Ministry of Education, Culture, Sports, Science and Technology and the Core Research for evolutionary Science and Technology (CREST) program of Japan Science and Technology Agency (JST).

References

- [1] S. Mutoh, T. Douseki, Y. Matsuya, T. Aoki, S. Sigematsu, and J. Yamada, *IEEE J. Solid-State Circuits*, vol. 30 (1995) 847-854.
- [2] H. Kawaguchi, K. Nose, T. Sakurai, in *IEEE ISSCC Dig. Tech. Papers*, vol. XLI, Feb. 1998, pp. 192-193.
- [3] M. Ishikawa, T. Kamei, Y. Kondo, M. Yamaoka, Y. Shimazaki, M. Ozawa, S. Tamaki, M. Furuyama, T. Hoshi, F. Arakawa, O. Nishi, K. Hirose, S. Yoshioka, and T. Hattori, *IEICE Trans. Electron.*, vol. E88-C (2004) 528-535.
- [4] Y. Kanno, H. Mizuno, Y. Yasu, K. Hirose, Y. Shimazaki, T. Hoshi, Y. Miyairi, T. Ishii, T. Yamada, T. Irita, T. Hattori, K. Yanagisawa, and N. Irie, *IEEE J. Solid-State Circuits*, vol. 42 (2007) 74-83.

- [5] S. Rusu, S. Tam, H. Muljono, D. Ayers, J. Chang, B. Cherkauer, J. Stinson, J. Benoit, R. Varada, J. Leung, R. D. Limaye, and S. Vora, *IEEE J. Solid-State Circuits*, vol. 42 (2007) 17- 25.
- [6] M. Yamaoka, Y. Shinozaki, N. Maeda, Y. Shimazaki, K. Kato, S. Shimada, K. Yanagisawa, and K. Osada, *IEEE J. Solid-State Circuits*, vol. 40 (2005) 186-194.
- [7] V. George, *Symp. High Performance Chips*, Aug. 2007, HC19.08.01.
- [8] T. Miwa, J. Yamada, H. Koike, H. Toyoshima, K. Amanuma, S. Kobayashi, T. Tatsumi, Y. Maejima, H. Hada, and T. Kunio, *IEEE J. Solid-State Circuits*, vol. 36 (2001) 522- 527.
- [9] S. Masui, T. Ninomiya, T. Ohkawa, M. Okura, Y. Horii, N. Kin, and K. Honda, *IEICE Trans. Electron.*, vol. E87-C (2004) 1769-1776.
- [10] W. Wang, A. Gibby, Z. Wang, T. W. Chen, S. Fujita, P. Griffin, Y. Nishi, and S. Wong, in *IEEE IEDM Tech. Dig.*, Dec. 2006, pp. 1-4.
- [11] M. Takata, K. Nakayama, T. Izumi, T. Shinmura, J. Akita, and A. Kitagawa, in *Abstr. IEEE 21st Nonvolatile Semiconductor Memory Workshop*, 2006, pp. 95-96.
- [12] S. Yuasa, T. Nagahama, A. Fukushima, Y. Suzuki, and K. Ando, *nature mater.*, vol. 3 (2004) 868-871.
- [13] S. S. P. Parkin, C. Kaiser, A. Panchula, P. M. Rise, B. Hughes, M. Samant, and S.-H. Yang, *nature mater.*, vol. 3 (2004) 862-867.
- [14] J. Hayakawa, S. Ikeda, F. Matsukura, H. Takahashi, and H. Ohno, *Jpn. J. Appl. Phys.*, vol. 44 (2005) L587-L589.
- [15] K. Inomata, *IEICE Trans. Electron.*, vol. E84-C (2001) 740-746.
- [16] S. Tehrani, J. M. Slaughter, M. Deherrera, B. N. Engel, . D. Rizzo, J. Salter, M. Durlam, R. W. Dave, J. Janesky, B. Butcher, K. Smith, and G. Grynkewich, *Proc. IEEE*, vol. 91 (2003) 703-714.
- [17] W. J. Gallagher and S. S. P. Parkin, *IBM J. Res. & Dev.*, vol. 50, (2006) 5-23.
- [18] D. Wang, M. Tondra, A. V. Pohm, C. Nordman, J. Anderson, J. M. Daughton, and W. C. Black, *J. Appl. Phys.*, vol. 87 (2000) 6385-6387.
- [19] K. J. Hass, G. W. Donohoe, Y.-K. Hong, and B. C. Choi, *IEEE Trans. Magn.*, vol. 42 (2006) 2751-2753.
- [20] W. Zhao, E. Belhaire, C. Chappert, and P. Mazoyer, *Proc. IEEE Computer Society Annu. Symp. VLSI*, 2008, p.40.
- [21] M. Hosomi, H. Yamagishi, T. Yamamoto, K. Bessho, Y. Higo, K. Yamane, H. Yamada, M. Shoji, H. Hachino, C. Fukumoto, H. Nagao, and H. Kano, in *IEEE IEDM Tech. Dig.*, Dec. 2005, pp. 459-462.
- [22] T. Kawahara, R. Takemura, K. Miura, J. Hayakawa, S. Ikeda, Y. Lee, R. Sasaki, Y. Goto, K. Ito, T. Megura, F. Matsukura, H. Takahashi, H. Matsuoka, and H. Ohno, *IEEE J. Solid-State Circuits*, vol. 43 (2008) 109-120.
- [23] G. D. Fuchs, N. C. Emley, I. N. Krivorotov, P. M. Braganca, E. M. Ryan, S. I. Kiselev, J. C.

- Sankey, D. C. Ralph, and R. A. Buhrman, *Appl. Phys. Lett.*, vol. 85 (2004) 1205-1207.
- [24] J. Hayakawa, S. Ikeda, Y. M. Lee, R. Sasaki, T. Meguro, F. Matsukura, H. Takahashi and H. Ohno, *Jpn. J. Appl. Phys.*, vol. 44 (2005) L1267-L1270.
- [25] H. Kubota, A. Fukushima, Y. Ootani, S. Yuasa, K. Ando, H. Maehara, K. Tsunekawa, D. D. Djayaprawira, N. Watanabe, and Y. Suzuki, *Jpn. J. Appl. Phys.*, vol. 44 (2005) L1237-L1240.
- [26] Y. Huai, D. Apalkov, Z. Diao, Y. Ding, A. Panchula, M. Pakala, L.-C. Wang, and E. Chen, *Jpn. J. Appl. Phys.*, vol. 45 (2006) 3835-3841.
- [27] Y. Fujimori, T. Nakamura, and H. Takasu, *Integrated Ferroelectrics*, vol. 47:1 (2002) 71-78.
- [28] K. Abe, S. Fujita, and T.H. Lee, in *Tech. Proc. 2005 NSTI Nanotechnology Conf. Trade Show*, vol. 3 (2005) 203-206.
- [29] S. Koyama, Y. Kato, T. Yamada, and Y. Shimada, *IEICE Trans. Electron.*, vol. E89-C (2006) 1368-1372.
- [30] S. Yamamoto and S. Sugahara: in preparation for publication.
- [31] W. Zhao, E. Belhaire, Q. Mistral, C. Chappert, V. Javerliac, B. Dieny, and E. Nicolle, in *Proc. Behavioral Modeling Simulation Conf. 2006*, vol. 1 (2006) 40-43.
- [32] Device Group at UC Berkeley, "Berkeley Predictive Technology Model," <http://www.eas.asu.edu/~ptm>.
- [33] S. Yamamoto and S. Sugahara: presented at 53rd Conf. Magnetism and Magnetic Materials, 2008, CT04.
- [34] S. Sugahara and M. Tanaka, *Appl. Phys. Lett.*, vol. 84 (2004) 2307-2309.
- [35] S. Sugahara, *IEE Proc. Circuits, Device-Systems*, vol. 152 (2005) 355-365.
- [36] S. Sugahara, *Physica Status Solidi C*, Vol. 3 (2006) 4405-4413.
- [37] S. Sugahara and S. Yamamoto: presented at 55th Spring Meet. Japan Society of Applied Physics, 2008, 30p-F-6.
- [38] Y. Shuto, S. Yamamoto, and S. Sugahara: to be published in *J. Appl. Phys.*

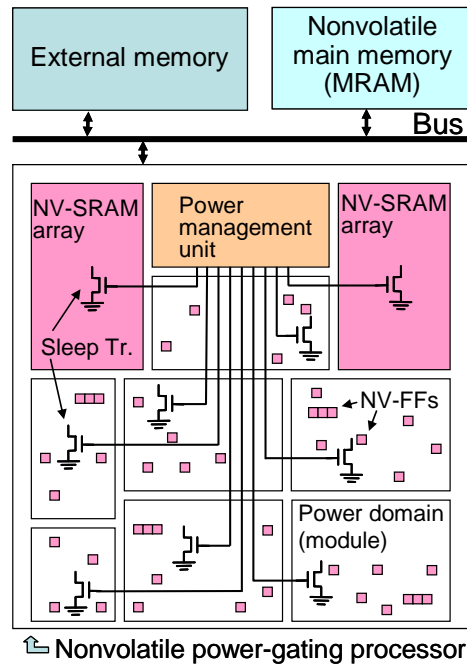


Fig. 1. Schematic illustration of nonvolatile power-gating processor. Combining nonvolatile main memory, a dynamically run-time power-gating computing system can be configured.

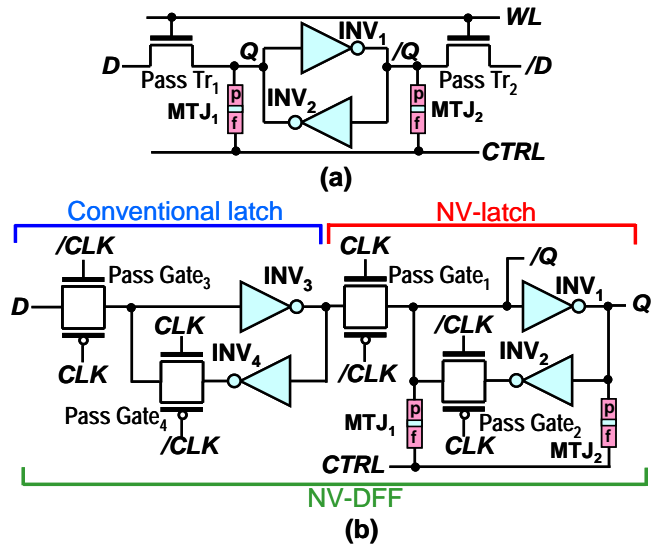


Fig. 2. Circuit configuration of the proposed (a) NV-SRAM cell and (b) positive edge triggered master-slave NV-DFF.

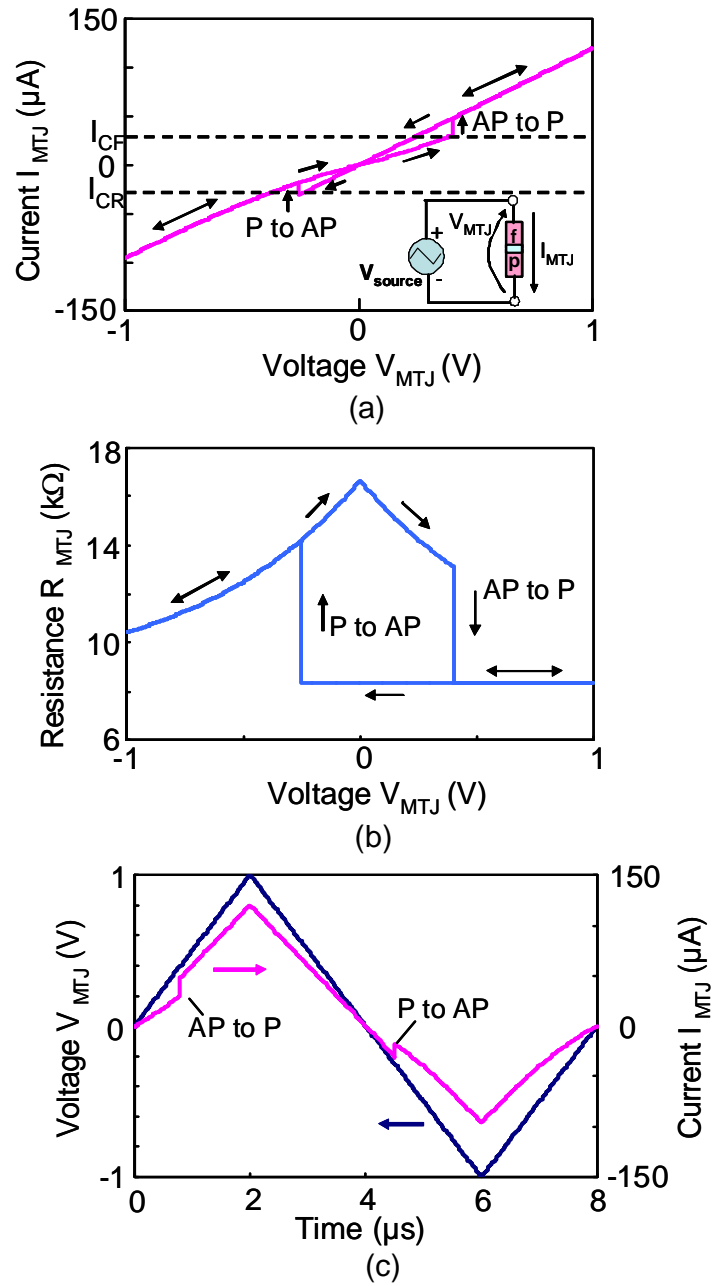


Fig. 3. (a) Current-voltage and (b) resistance-voltage characteristics of the present MTJ model. The current direction is shown in the inset, where f and p denote the free and pinned layers of the MTJ model, respectively. P and AP in the figure indicate the parallel and antiparallel magnetization configurations, respectively. (c) Simulated response of the MTJ current, when an alternating triangle voltage is applied to the MTJ model.

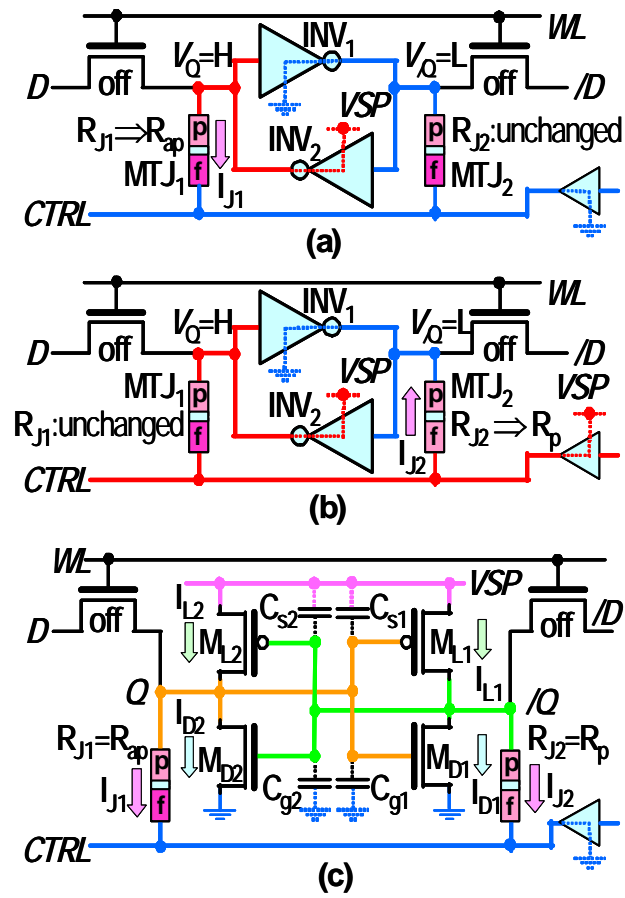


Fig. 4. Schematic illustrations of store operation with (a) level L and (b) level H voltages on the CTRL line. (c) Schematic illustration of restore operation, where M_{L1} (M_{L2}) and M_{D1} (M_{D2}) configure INV_1 (INV_2).

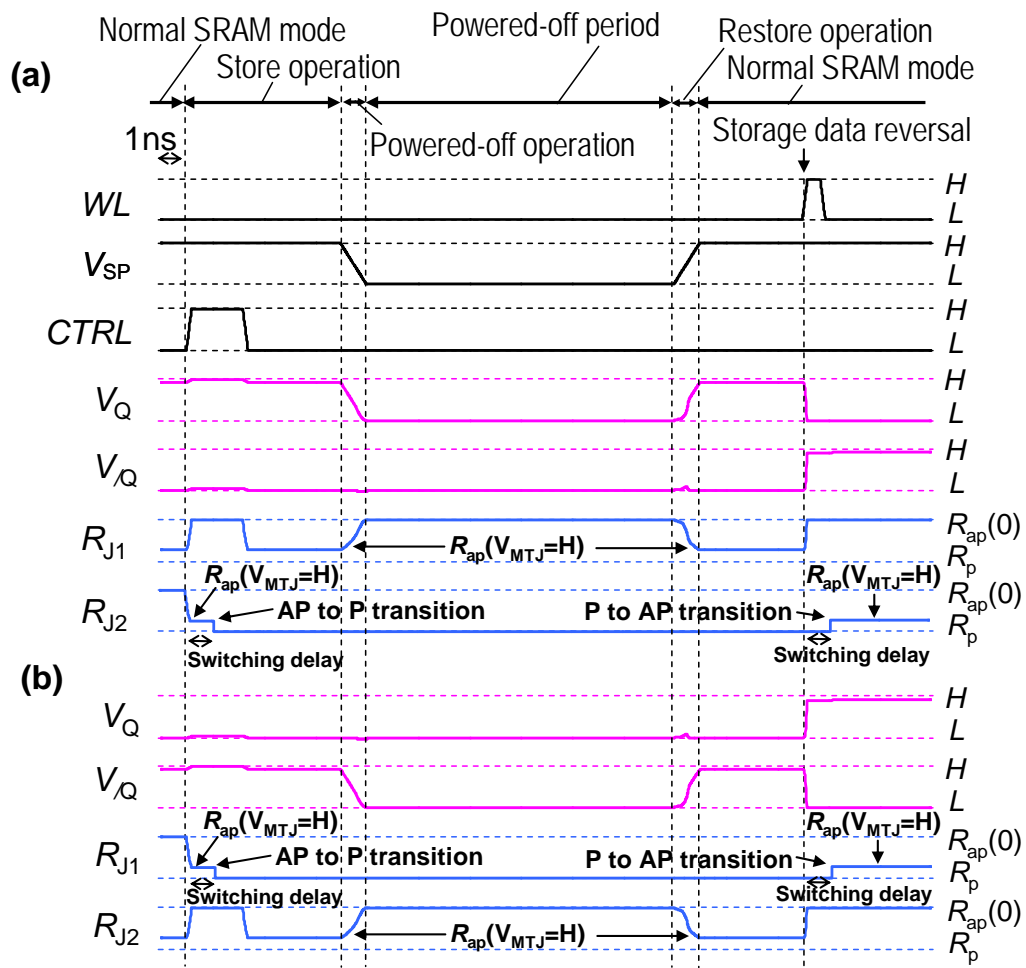


Fig. 5. Simulated input and output waveforms of the NV-SRAM cell for the store, restore, and normal SRAM mode operations with initial conditions of (a) $V_Q=H$ and $V_{\bar{Q}}=L$ and (b) $V_Q=L$ and $V_{\bar{Q}}=H$.

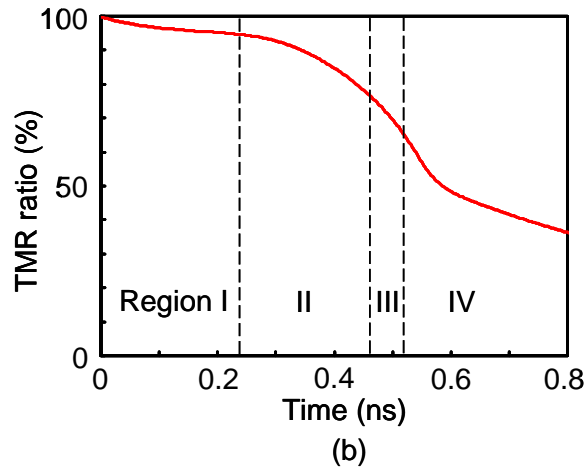
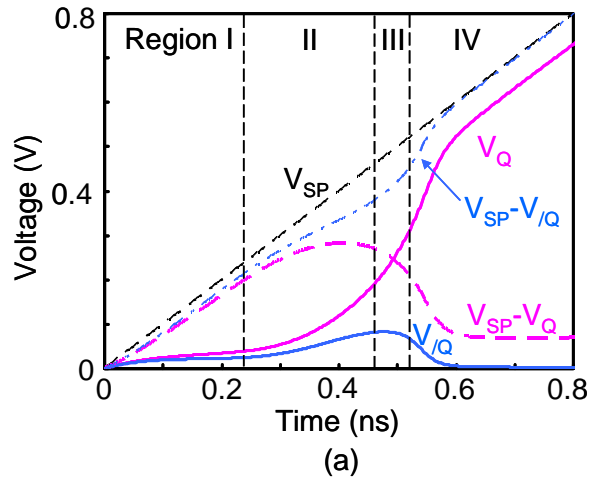


Fig. 6. (a) Time evolution of the node voltages V_Q and V_Q , and their differences with respect to V_{SP} . (b) TMR ratio of MTJ_1 during the restore operation.

